

# A new image analysis algorithm for contact angle measurement at high temperature

Krzysztof Strzecha 

Institute of Applied Computer Science, Lodz University of Technology, Lodz, Poland

E-mail: [strzecha@iis.p.lodz.pl](mailto:strzecha@iis.p.lodz.pl)

Received 11 July 2019, revised 23 October 2019

Accepted for publication 30 October 2019

Published 31 December 2019



## Abstract

In recent years there has been considerable progress in automated techniques for measuring basic parameters characterizing interfacial interaction. However, the existing automated measurement systems can only measure properties of selected materials in a narrow temperature range. Also, the existing image processing and analysis algorithms are sensitive to interference and require precise positioning of the specimen. It is particularly difficult to use the algorithms to measure the specimen at high temperature, because the quality of acquired images is affected not only by the imperfection of the vision subsystem but also by the distortion due to the flow of protective gases. This paper presents a new image analysis algorithm, which has been developed for fully automatic measurement of the contact angle in a wide temperature range for a variety of materials. The measurement is based on successive approximation of the specimen edge with ellipses. The algorithm has been implemented in a system, which can measure surface tension and wetting angle, and tested in a wide temperature range for a variety of specimen materials. This algorithm has a number of advantages over the existing ones, in particular immunity to the shape, size and location of the specimen and low computational cost. The obtained results are independent of the subjective assessment of the measuring system operator with high reproducibility.

Keywords: image segmentation, image analysis, contact angle, high temperature

(Some figures may appear in colour only in the online journal)

## 1. Introduction

In many industrial processes, there exist interfaces between liquid, gas and solid state, e.g. in welding, making of composite materials with liquid, sintering of powders, saturation of porous structures, coating, refining of metals to eliminate non-metallic inclusions, foundry or processes of crystallization from a liquid phase. While it is important to understand the phenomena occurring at the interfaces, the knowledge of physical-chemical processes occurring between liquid, gas and solid state is limited.

A number of monographs and review papers have pointed out the significance of the phenomena at the interfaces in different fields [1–4]. The related theory of surface phenomena physics and measurement methods can be found in many publications [4–8].

The basic measurable quantities for characterizing surface interaction include the surface tension of the liquid phase and the extreme angle of wetting of the base by a liquid. It is common to perform measurements and calculations based on thermodynamic equilibrium. In many cases, however, the equilibrium cannot be reached or can be reached after very long time, e.g. diffusion processes, dissolution of the base in the liquid phase, formation of new chemical compounds or inter-metallic phases. In such cases, it is crucial to measure dynamic, time-variable quantities, possibly in combination with a structural analysis of the interfacial boundary.

To investigate the interfacial processes occurring in the solid–liquid or liquid–liquid systems of two different materials, there are a few challenges: the activity of the materials in the liquid state, the need for precisely controlled atmosphere composition, the sensitivity to contamination, and carrying

out measurements at high temperature. In many cases, it is necessary to track changes of interfacial processes in transient states, e.g. at the interface of the molten metal and slag substances in steel metallurgy.

The fundamental techniques for determination of the wetting angle and surface tension are optical methods, which are based on continuous observation of the specimen shape and the manual or photographic recording of changes in its profile as a function of temperature. The recorded profiles are analysed by a qualified specialist using graphical methods, to measure the basic parameters of the droplet and then the values of the parameters are calculated. This type of measurement system has a number of drawbacks: extremely labour-intensive, strenuous measurement, and effect of the human factor on the measurement results.

The algorithms used to measure the contact angles can be divided into two groups: tensometric method and goniometric method. The tensometric method is based on the following Young equation and determining the contact angle when the surface tension values are known by other methods.

$$|\bar{\sigma}_{LV}| \cos\theta + |\bar{\sigma}_{SL}| - |\bar{\sigma}_{SV}| = 0; \quad (1)$$

where  $\theta$  is the wetting angle;  $|\bar{\sigma}_{SV}|$  is the surface tension on the border of solid–gas;  $|\bar{\sigma}_{SL}|$  is the surface tension on the border of solid–liquid; and  $|\bar{\sigma}_{LV}|$  is the surface tension on the border of liquid–gas.

The main disadvantage of this method is that it can only be used to measure symmetrical droplets. In practice, their use proves to be very limited due to substrate heterogeneities, roughness or adsorption.

The goniometric method is based on analysis of droplet shape using specialized algorithms for processing and analysis of digital images. The axisymmetric drop shape analysis (ADSA) method is well known and often used as a [9]. Other methods try to describe the shape of a specimen with a circle [10] or an ellipse [11]. Similar to ADSA, they can only be used for symmetrical droplets. In most cases, however, the specimen is not symmetrical. Therefore, it is necessary to search for algorithms that can measure non-axisymmetric droplets.

In the past few years, a number of such methods have been proposed, including polynomial fitting [12], sub-pixel polynomial fitting [13], moving goniometric mask [14], and 3D analysis [15]. Several such methods, including secant one, polynomial edge fitting, contour analysis and gradient intensity statistics were reviewed [16].

In recent years there has been considerable progress in automated techniques for measuring basic parameters for characterizing interfacial interaction. Several systems can measure the extreme wetting angle and the surface tension of liquid metals and solids in a protective atmosphere. Some fully automated measurement systems can only measure properties of selected materials in a narrow temperature range. Also, the image processing and analysis algorithms implemented in those systems are sensitive to interference and require precise positioning of the specimen. There are some commercial solutions [17]. Unfortunately, their manufacturers do not provide any specific information on the applied image processing

algorithms and analysis. In addition, commercial devices are very expensive and not easily accessible.

The author was involved in developing an automatic system for measuring the extreme angle and surface tension of liquid metal and solids in a wide range of temperature in a protective atmosphere [18–20]. The algorithms used in the system for image processing and analysis are based on the sessile drop technique [4, 8]. The image analysis algorithm developed allows for fully automatic measurement of the contact angle in a wide temperature range for a variety of materials. It also allows analysis of non-axisymmetric droplets. The measurement is based on successive approximations of the specimen edge with ellipses.

It should be remembered that the problem of automated contact angle measurement is not only the approximation of the edge of the droplet, but also the entire process of pre-processing the image and edge detection. In particular, stages of correct and precise detection of drop edges are not fully solved. Well known methods work fine only for a limited temperature range, drop shape and lighting condition [16, 17, 21–23]. The proposed method tries to solve these problems by combining edges detection with their approximation. As the result, the proposed method offers a fully automated measuring process, independent of any subjective assessment of the operator and gives stable (low standard deviation) results regardless of the measurement temperature, lighting conditions and protective atmosphere gas flows.

## 2. Sessile drop method and measurement system

The shape of the drops placed on a non-wettable surface depends on two types of forces: the surface tension, which attempts to give a droplet a spherical shape, and the gravity by which the drop is ‘flattened’. In the case of the spherical drops, it is difficult to determine the surface tension. When the effect of gravity is comparable with the effect of surface energy, the surface tension can be determined. The equatorial diameter of the metal droplets should be practically at least 0.5 cm. The distortion occurring in a spherical droplet allows us to determine the surface tension based on the droplet dimensions and physical constants. However, only symmetric drops can be taken into account [4, 8].

To determine the contact angle, a direct measuring method is based on the point of contact of the three phases.

An automated system for measuring surface phenomena occurring in contact of liquid and solid phases is shown in figure 1 [20, 24]. This system is named THERMO-WET, which can measure the surface tension of a liquid and the wetting angle of a solid by a liquid.

The parameters are determined using the sessile drop method under the conditions of thermodynamic equilibrium, and in the case of transient states as a function of time and temperature. Tests may be conducted in a controlled atmosphere, in a temperature range of up to 1800 °C, for interfacial solid–liquid systems of two different materials. The measurement process takes place using specially designed algorithms for processing and analysis of images, which are obtained

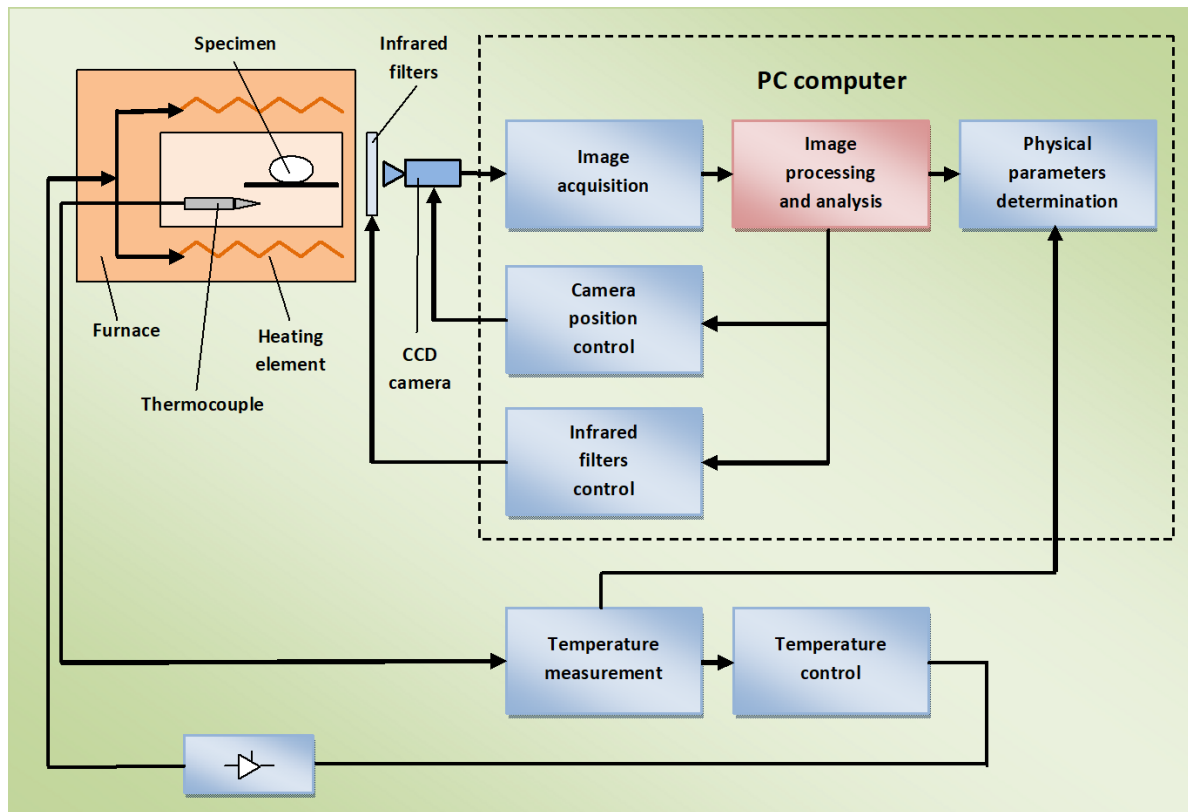


**Figure 1.** Block diagram of THERMO-WET system for measuring surface phenomena occurring in contact of liquid and solid phases designed and built in Institute of Applied Computer Science of Lodz University of Technology.

from a camera observing a sample of the test material placed inside a high-temperature furnace. The measurement results are characterized with high accuracy and high reproducibility, compared with those obtained by previous methods, which are time-consuming and depend on the operator's subjective assessments.

The measurement system (figure 1) consists of a two zone high-temperature electric furnace equipped with a high-precision temperature controller, a process gases supply system, a system for loading and discharge of the specimen, a CCD camera coupled with the computer controlling the measurement process, and specialized programs for image processing and analysis, data processing, editing and archiving of results [20, 24].

Image processing and analysis algorithms developed for the THERMO-WET system can be divided into the following three groups: (1) image enhancement algorithms; (2) image segmentation algorithms; and (3) algorithms for precise measurement of specimen geometrical properties.

It is difficult to process and analyse the images obtained at high temperature because the quality of the acquired images is affected not only by imperfections of the vision subsystem but also by the distortion brought by the flow of protective gases. All of them lead to significant ambiguities in the precise location of the edges of the specimen. The influences of the vision system imperfections and the methods of its corrections were considered in details in [20, 25]. For most materials, measurements of the wetting angle are carried out in a protective atmosphere. The flow of protective gas introduces

significant distortions to the acquired images [20, 26]. Gas, of a temperature of approximately 0 °C, is introduced to the furnace chamber from the side of the CCD camera and then, on its way to the specimen, it is heated to the current working temperature of, for example, 1500 °C. The absolute index of the light refraction in gas depends on its density and temperature. In the given example its value decreases nearly 40 times (according to Boyle–Mariotte's law). Hence, it can be assumed that the gas introduced to the furnace should be considered the optical lens, whose index of light refraction smoothly changes between the camera and the specimen. Phenomena related to gas flow in the furnace chamber and suggestions for correction of the distortions introduced by them are discussed in [20, 24, 26].

Another important problem is the sensitivity of commonly used edge detection methods to lighting conditions. These conditions change significantly with increasing temperature in the furnace chamber or when changing optical filters, which are often used to limit the amount of light reaching the photo-sensitive element of the camera. There is still a need to search for algorithms that give reproducible measurement results in different lighting conditions.

### 3. Measurement of contact angle

As mentioned above, specialized image processing and analysis algorithms are used in the THERMO-WET system. Figure 2 shows a flowchart of an algorithm for measuring the

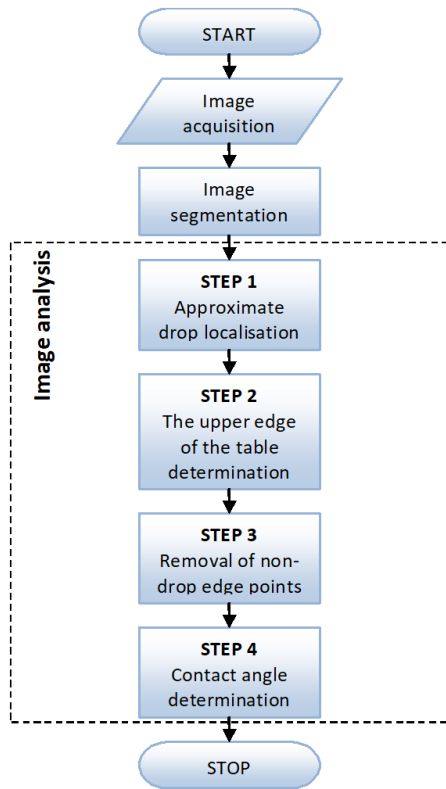


**Figure 2.** Flowchart of algorithm for determining contact angles. The image analysis process consists of four stages: (1) drop localization, (2) determination of upper edge, (3) removal of non-drop edge points, and (4) determination of contact angle.

contact angles, including three stages: (1) image acquisition, (2) image segmentation and (3) image analysis.

The THERMO-WET system can acquire monochrome 8-bit digital images, using the CCD camera, with a resolution of  $1280 \times 1024$ . Figures 3(a) and 4(a) show typical images obtained during the measurement processes. Figure 3(a) shows a specimen of copper (Cu) on  $\text{Al}_2\text{O}_3$  plate at temperature  $1195^\circ\text{C}$ . Figure 4(a) shows a specimen of glass ( $\text{SiO}_2$ —35%,  $\text{PbO}$ —59%,  $\text{K}_2\text{O}$ —6%) on the  $\text{Al}_2\text{O}_3$  plate at temperature  $885^\circ\text{C}$ .

### 3.1. Image segmentation

The purpose of segmentation is to divide a set of points on a digital image to disjoint subsets that meet certain criteria for homogeneity (e.g. colour, brightness, and texture). Each of these subsets has a specific meaning in relation to the characteristics of the observed scene. Although different segmentation techniques are developed [27, 28], there is no general theory of segmentation. For the THERMO-WET system, various segmentation algorithms are theoretically analysed and experimentally verified [19]. Initial image segmentation is performed using well-known algorithms [29], including histogram stretching, Gaussian blur and Canny edge detection [30].

Segmentation result is an unordered set of all edge points of an image. Images of specimens shown in figures 3(a) and

4(a) with marked sets of detected edge points are shown in figures 3(b) and 4(b) respectively.

### 3.2. Image analysis

Image analysis is a process of creating a quantitative description of the recorded scene, according to an established model of the scene and an optical system. The model should take into account the relationship between the distribution of the intensity of the light in the registered scene containing objects of the considered classes, and the brightness of the digital image. It should also take into account all these side effect factors associated with the imperfection of the camera and electronic components of the vision system that may have a negative effect on the accuracy of image feature measurement.

Input data for image analysis algorithms is a set of edge points detected during the segmentation process. The analysis process to determine the contact angles, as shown in figure 2, consists of four stages: (1) drop localization, (2) determination of upper edge, (3) removal of non-drop edge points, and (4) determination of contact angle.

**3.2.1. Drop localization.** The aim of this stage is to determine the approximate drop position in the registered scene and to roughly determine its size and shape. Its results will allow us to clean the analysed image from non-drop edge points and to remove the artifact appearing inside the specimen. After this step, it is possible to extract the edge points representing the upper edge, on which the drop is located.

To determine the approximate position and shape of the drop, ellipse matching of a set of detected edge points is used. First, circles are adjusted to the left and right half-profiles of the drop. Then the length of the major axis of the searched ellipse is determined. It is expressed as the distance between the centres of the found circles, increased by their radii. This solution significantly speeds up the entire ellipse fitting process, which is limited to determining the length of its minor axis and its centre. The results of the approximate localization of the specimens in figures 3(a) and 4(a) are shown in figures 3(c) and 4(c) respectively. The circles matching left and right half-profiles are marked in red, and the ellipses found are marked in blue.

**3.2.2. Determination of upper edge.** This stage starts with original image filtration using vertical Sobel masks [29]. The next step is to remove all points not belonging to the edge of the solid (including those representing the edge of the drop), from the filtered image. Having determined the parameters of the ellipse in the previous stage, the edge points lying above the ellipse and inside it are removed. In the end, a row with the maximum gradient value is determined for each column of the image. The position of the upper edge of the solid surface is determined by the row, for which the highest number of maximum gradient values has been found. The results of the upper edge of the solid surface (marked in red) determination in the images from figures 3(a) and 4(a) are shown in figures 3(d) and 4(d) respectively.

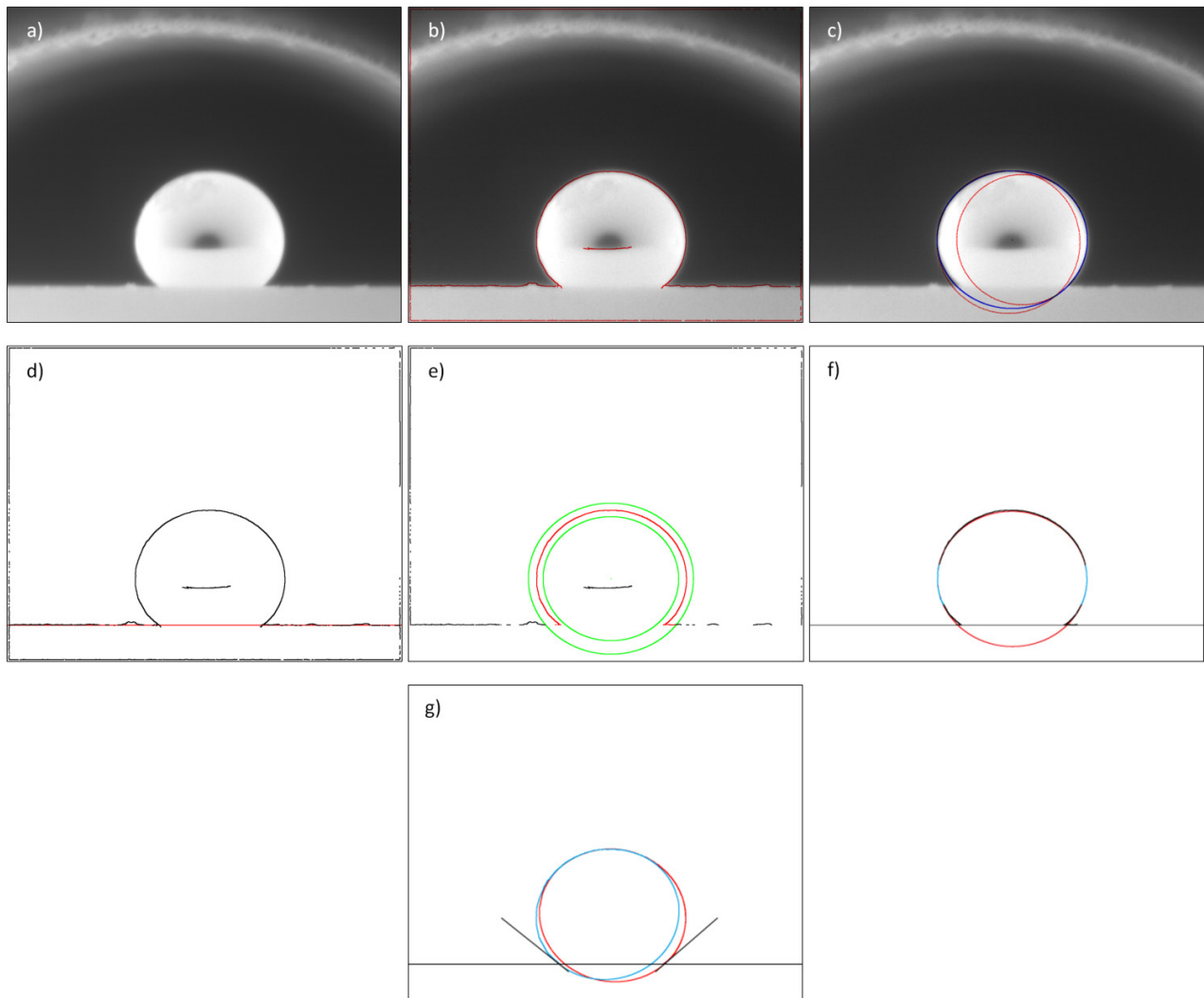


**Figure 3.** Image of a copper specimen (Cu) on  $\text{Al}_2\text{O}_3$  plate at  $1195\text{ }^\circ\text{C}$  obtained during the measurement processes and the steps of its processing: (a) original image, (b) segmentation result, set of detected edge points is marked in red, (c) approximate localization of specimen, the circles matching left and right half-profiles are marked in red, and the ellipse found is marked in blue, (d) determination of upper edge of the solid surface (marked in red), (e) result of the first step of non-drop edge points removal, determined ellipses are marked in green and removed edge points are marked in black, (f) approximation with an ellipse to eliminate distortion of edge points in area of contact of three phases, sets of approximated edge points are marked in blue and the determined ellipse is marked in red, (g) final result of determination of contact angle, ellipses approximating profiles are marked red and blue and their tangents at points of their intersection with the edge of table are marked in black.

**3.2.3. Removal of non-drop edge points.** This stage has two steps: (1) preliminary removal of non-drop points, and (2) removal of drop edge artifacts and distortion points in the three phase contact area. In the first step, points located inside the ellipse of 10% smaller and outside the ellipse by 10% greater than the one determined in the first stage of the analysis are removed from the set of detected edge points. The results are presented in figures 3(e) and 4(e) for the images in figures 3(a) and 4(a) respectively. The determined ellipses are marked in green and removed edge points are marked in black.

Due to strong light emission by the heated drop and the table, edges obtained as a result of segmentation are strongly distorted in the area of contact of three phases (see figure 5). The distortion smoothly passes into the line of the upper edge

of the table, making it difficult to accurately determine the place where it begins and ends. Only a precise distinction of the drop edge points from the distortion points enables further correct analysis of the drop shape. To detect droplet edge distortion the algorithm uses iterative approximations of edge points with an ellipse. Then the set is supplemented with another edge point and the next approximation is performed. The quality of approximation for the new set is evaluated in relation to the approximation of the previous set. The given point is recognized as belonging to the edge or to distortion.

The results of the approximation with an ellipse to eliminate distortion of the edge points in the area of contact of three phases for images in figures 3(a) and 4(a) are shown in figures 3(f) and 4(f) respectively. The sets of approximated

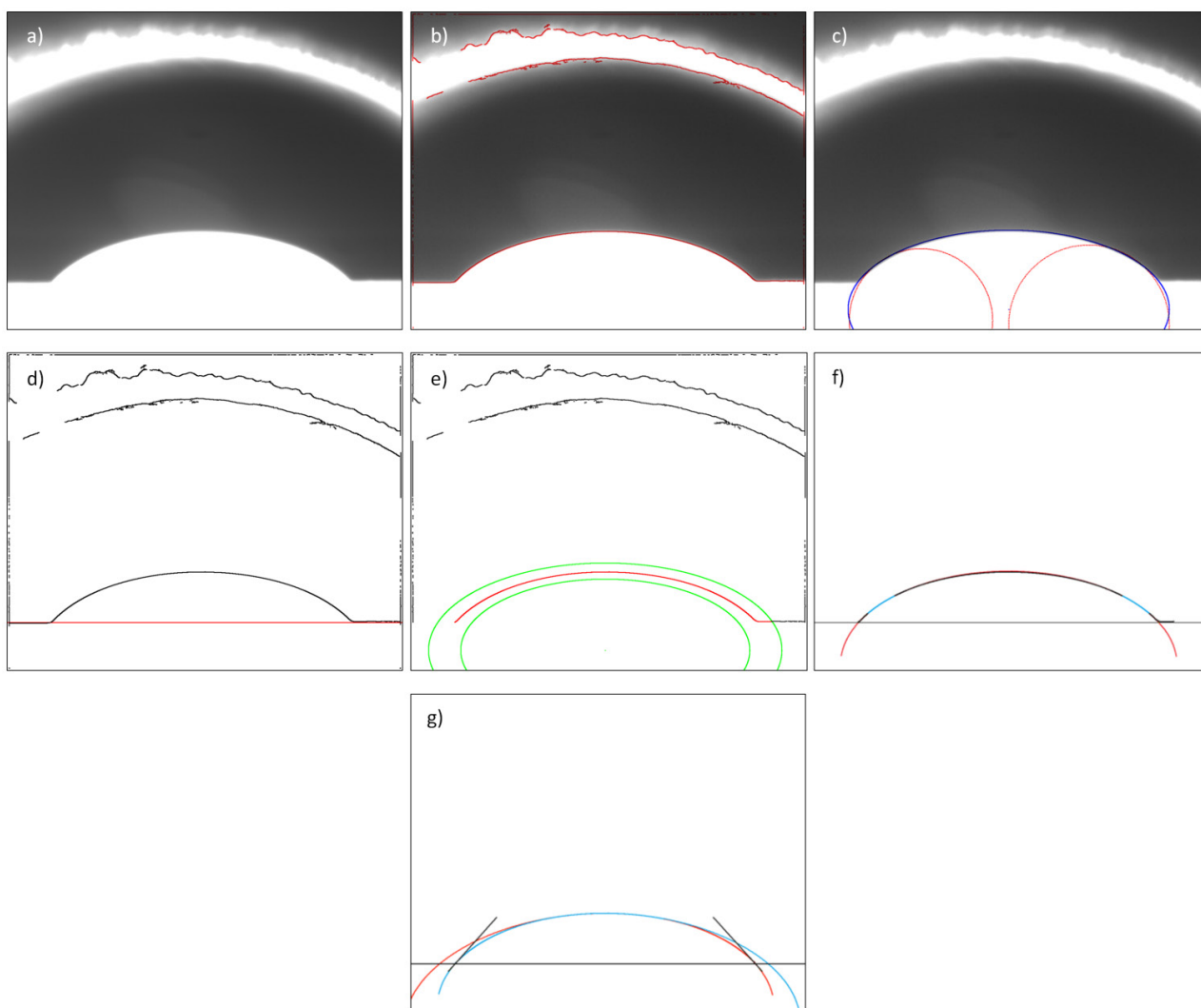


**Figure 4.** Image of a glass specimen ( $\text{SiO}_2$ —35%,  $\text{PbO}$ —59%,  $\text{K}_2\text{O}$ —6%) on  $\text{Al}_2\text{O}_3$  plate at 885 °C obtained during the measurement processes and the steps of its processing: (a) original image, (b) segmentation result, set of detected edge points is marked in red, (c) approximate localization of specimen, the circles matching left and right half-profiles are marked in red, and the ellipse found is marked in blue, (d) determination of upper edge of the solid surface (marked in red), (e) result of the first step of non-drop edge points removal, determined ellipses are marked in green and removed edge points are marked in black, (f) approximation with an ellipse to eliminate distortion of edge points in area of contact of three phases, sets of approximated edge points are marked in blue and the determined ellipse is marked in red, (g) final result of determination of contact angle, ellipses approximating profiles are marked red and blue and their tangents at points of their intersection with the edge of table are marked in black.

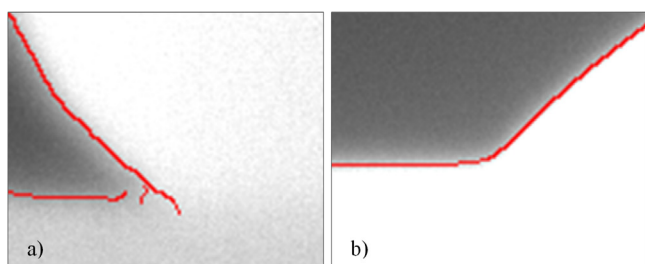


**Figure 5.** Distortions in areas of contact of three phases in images of: (a) Cu on  $\text{Al}_2\text{O}_3$ , (enlarged fragment of image in figure 3(a)), (b) glass on  $\text{Al}_2\text{O}_3$  (enlarged fragment of image in figure 4(a)).

edge points are marked in blue and the determined ellipses are marked in red. The presented method can identify and eliminate all kinds of distortion by further analysis.

**3.2.4. Determination of contact angle.** To determine the contact angle, a tangent function describing the profile of the drop at the point of its intersection with the upper plane of the solid phase is calculated. Due to the drop shape, it is difficult to approximate its whole edge with one function. It is possible, however, to approximate with an ellipse, separately the points of the right and left half-profiles of the drop. For both half-profiles, the point of ellipse intersection with the upper edge of the solid surface is determined. The final step is to calculate the contact angle as the angle of tangent inclination to the edge of the surface. Figures 3(g) and 4(g) show the results of determination of the contact angles for specimens in figures 3(a) and 4(a) respectively. The ellipses approximating both profiles (red and blue) and their tangents at points of their intersection with the upper edge of table (marked in black) are presented.

**Table 1** Left half-profile contact angle measurement results in Cu on Al<sub>2</sub>O<sub>3</sub> experiment.

<i>T</i> (°C)	Proposed method			ADSA		LB-ADSA		Ellipse (best-fit)		Ellipse (manual)	
	$\theta_L$ (°)	$d_L$ (°)	Confidence interval (°)	$\theta_L$ (°)	$d_L$ (°)	$\theta_L$ (°)	$d_L$ (°)	$\theta_L$ (°)	$d_L$ (°)	$\theta_L$ (°)	$d_L$ (°)
1135	141.42	0.568	(141.22, 141.62)	142.00	0.100	139.04	3.940	132.68	1.292	140.53	0.977
1145	141.12	0.545	(140.92, 141.31)	139.97	0.153	144.08	1.433	132.40	1.051	141.08	0.960
1155	141.08	0.369	(140.95, 141.21)	138.03	0.174	142.45	1.382	132.55	0.862	141.83	1.884
1165	140.50	0.698	(140.25, 140.75)	136.73	0.161	140.96	3.937	131.95	0.954	141.23	0.852
1175	141.27	0.514	(141.08, 141.45)	134.57	0.404	144.81	1.131	131.87	0.882	141.28	0.755
1185	140.52	0.466	(140.35, 140.69)	132.20	0.200	142.06	4.545	132.27	0.946	141.97	0.816
1195	141.48	0.584	(141.27, 141.69)	130.90	0.346	144.70	3.347	133.52	1.013	142.27	0.781
1205	141.34	0.367	(141.21, 141.47)	128.60	0.141	143.79	1.520	139.65	1.181	142.47	0.769
1215	141.14	0.333	(141.02, 141.26)	133.77	0.231	143.03	5.032	136.32	0.950	142.27	0.753
1225	141.24	0.429	(141.09, 141.40)	131.55	0.071	143.99	2.130	132.13	0.665	142.22	0.926
1235	140.34	0.330	(140.23, 140.46)	129.33	0.321	142.57	0.444	134.97	0.882	140.85	0.929

**Table 2.** Right half-profile contact angle measurement results in Cu on Al<sub>2</sub>O<sub>3</sub> experiment.

<i>T</i> (°C)	Proposed method			ADSA		LB-ADSA		Ellipse (best-fit)		Ellipse (manual)	
	$\theta_R$ (°)	$d_R$ (°)	Confidence interval (°)	$\theta_R$ (°)	$d_R$ (°)	$\theta_R$ (°)	$d_R$ (°)	$\theta_R$ (°)	$d_R$ (°)	$\theta_R$ (°)	$d_R$ (°)
1135	138.09	0.412	(137.94, 138.23)	140.93	0.058	139.04	3.940	132.00	1.483	139.15	1.027
1145	138.17	0.414	(138.02, 138.32)	139.37	0.231	144.08	1.433	131.45	1.183	140.10	0.769
1155	138.25	0.479	(138.08, 138.42)	137.80	0.100	142.45	1.382	131.97	0.797	141.42	2.009
1165	138.41	0.425	(138.26, 138.56)	136.30	0.120	140.96	3.937	131.17	0.958	140.35	1.033
1175	138.02	0.439	(137.86, 138.17)	134.33	0.351	144.81	1.131	131.18	0.850	140.45	0.362
1185	137.38	0.507	(137.19, 137.56)	132.50	0.131	142.06	4.545	131.75	0.931	141.25	1.035
1195	138.43	0.449	(138.27, 138.59)	130.53	0.451	144.70	3.347	133.23	0.995	141.55	0.971
1205	138.61	0.341	(138.49, 138.74)	128.15	0.354	143.79	1.520	138.57	1.297	141.70	0.963
1215	137.60	0.335	(137.48, 137.72)	134.67	0.058	143.03	5.032	135.72	0.893	141.15	0.822
1225	137.77	0.365	(137.64, 137.90)	133.40	0.141	143.99	2.130	131.85	0.582	141.27	1.402
1235	138.12	0.280	(138.02, 138.22)	132.17	0.451	142.57	0.444	135.67	0.712	140.50	0.876

**Table 3.** Left half-profile contact angle measurement results in glass on Al<sub>2</sub>O<sub>3</sub> experiment.

<i>T</i> (°C)	Proposed method			ADSA		LB-ADSA		Ellipse (best-fit)		Ellipse (manual)	
	$\theta_L$ (°)	$d_L$ (°)	Confidence interval (°)	$\theta_L$ (°)	$d_L$ (°)	$\theta_L$ (°)	$d_L$ (°)	$\theta_L$ (°)	$d_L$ (°)	$\theta_L$ (°)	$d_L$ (°)
775	90.35	0.452	(90.19, 90.51)	90.37	0.651	90.58	0.991	91.83	3.931	89.43	0.808
785	84.17	0.486	(84.00, 84.36)	83.53	0.702	90.57	2.062	88.13	1.914	84.83	2.159
795	76.10	0.409	(75.96, 76.25)	75.37	0.862	—	—	80.60	1.646	75.83	2.113
805	70.01	0.337	(69.88, 70.13)	63.70	5.551	—	—	76.40	0.458	70.73	1.457
815	65.67	0.376	(65.53, 65.80)	56.47	6.882	—	—	71.07	5.727	67.83	2.635
825	61.19	0.266	(61.10, 61.29)	59.93	0.321	—	—	72.63	0.153	61.03	0.208
835	57.02	0.366	(56.89, 57.15)	55.23	0.651	—	—	71.07	3.361	55.47	1.450
845	54.26	0.307	(54.15, 54.37)	52.05	0.212	—	—	71.80	1.249	54.03	2.250
855	52.69	0.324	(52.57, 52.80)	49.90	0.707	—	—	73.50	2.787	53.63	1.069
865	50.99	0.293	(50.88, 51.09)	47.93	0.351	—	—	71.93	2.684	52.17	2.608
875	49.68	0.316	(49.57, 49.79)	46.67	0.252	—	—	73.03	5.472	49.50	1.646
885	48.08	0.318	(47.97, 48.20)	41.60	4.530	—	—	65.53	2.335	50.15	2.335
895	47.26	0.329	(47.14, 47.38)	43.73	0.351	—	—	72.30	6.180	47.47	1.350

**4. Measurement results**

The algorithm for determining contact angles presented in the previous section has been tested in a wide temperature range for a variety of specimen materials. The results of experiments with copper (Cu) and glass (SiO<sub>2</sub>—35%, PbO—59%,

K<sub>2</sub>O—6%) specimens are presented. In both cases specimens were located on Al<sub>2</sub>O<sub>3</sub> surface. The contact angle was measured independently for the left and right half-profiles of the specimen. The obtained results are listed in tables 1 and 2 (copper) and tables 3 and 4 (glass), where *T* is the specimen temperature;  $\theta_L$  and  $\theta_R$  are the average value of measured

**Table 4.** Right half-profile contact angle measurement results in glass on Al<sub>2</sub>O<sub>3</sub> experiment.

<i>T</i> (°C)	Proposed method			ADSA		LB-ADSA		Ellipse (best-fit)		Ellipse (manual)	
	$\theta_R$ (°)	$d_R$ (°)	Confidence interval (°)	$\theta_R$ (°)	$d_R$ (°)	$\theta_R$ (°)	$d_R$ (°)	$\theta_R$ (°)	$d_R$ (°)	$\theta_R$ (°)	$d_R$ (°)
775	91.73	0.481	(91.56, 91.90)	94.20	1.253	90.58	0.991	95.17	3.372	91.00	2.166
785	85.11	0.627	(84.88, 85.33)	85.30	0.800	90.57	2.062	88.30	0.917	85.60	1.800
795	76.60	0.550	(76.40, 76.80)	75.83	1.069	—	—	80.60	1.493	76.53	2.458
805	70.55	0.333	(70.43, 70.67)	69.87	0.513	—	—	75.63	0.723	69.30	2.300
815	66.01	0.334	(65.89, 66.13)	60.40	6.505	—	—	70.50	5.647	66.53	1.550
825	61.99	0.455	(61.83, 62.15)	60.10	0.656	—	—	72.77	1.343	63.63	0.757
835	57.74	0.584	(57.53, 57.95)	54.53	0.451	—	—	70.97	3.009	55.77	2.515
845	54.71	0.420	(54.55, 54.86)	50.80	0.693	—	—	70.30	2.193	53.50	1.609
855	52.96	0.362	(52.83, 53.09)	46.50	5.122	—	—	71.97	3.179	52.40	0.900
865	51.09	0.427	(50.93, 51.24)	47.27	0.153	—	—	67.40	2.651	51.87	3.201
875	49.66	0.460	(49.50, 49.82)	40.97	8.808	—	—	70.63	5.960	49.77	1.115
885	47.87	0.479	(47.70, 48.04)	40.70	5.444	—	—	64.73	3.612	49.31	3.612
895	47.04	0.362	(46.91, 47.17)	40.83	4.277	—	—	72.50	6.426	47.83	2.113

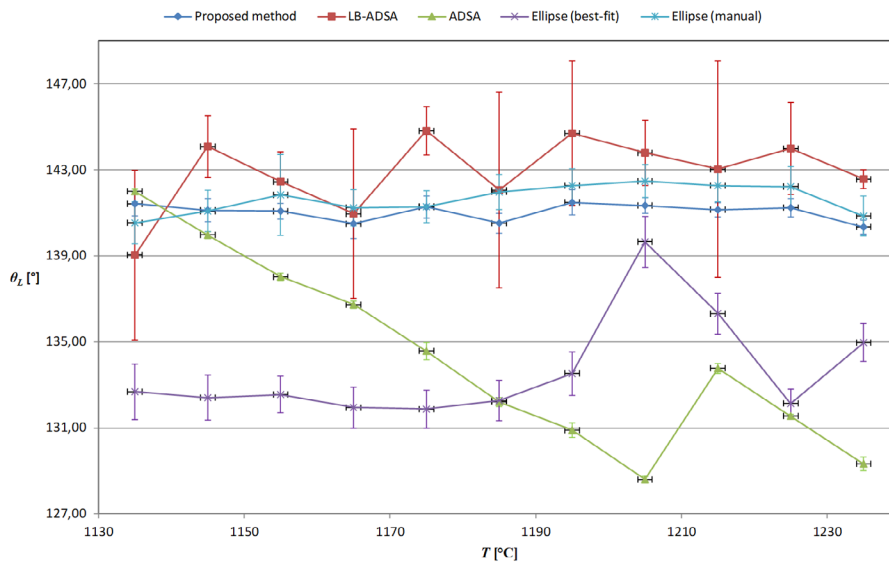


**Figure 6.** Average values of contact angles for left half-profiles measured in Cu on Al<sub>2</sub>O<sub>3</sub> experiment as function of temperature.

contact angle, left and right respectively; and  $d_L$  and  $d_R$  are the standard deviation of measured contact angle, left and right respectively.

The proposed algorithm was implemented in the C++ programming language. All calculations were performed on the PC equipped with an Intel i7 processor clocked at 2.4 GHz and 8 GB of RAM. The processing time for a single image was 5 s and was independent of the sample shape. The method allows for fully automated measurement without operator participation.

**4.1. Cu on Al<sub>2</sub>O<sub>3</sub>**

The material of the specimen was copper (Cu) and the material of the substrate was Al<sub>2</sub>O<sub>3</sub>. The measurements were carried out in the temperature range 1135 °C–1235 °C with a step of 10 °C. Thirty images were obtained for each temperature. Independent measurements of contact angles were made for each of them. Tables 1 and 2 present average values of the

measured angles for individual temperature and their standard deviations, for left and right half-profiles respectively. Confidence intervals were calculated for average values of the contact angles for every temperature and presented as well. Confidence level was assumed to be 95%. Figure 6 shows the average values of the contact angles for left half-profiles and figure 7 shows the average values of the contact angles for right half-profiles as functions of temperature.

**4.2. Glass on Al<sub>2</sub>O<sub>3</sub>**

The material of the specimen was glass (SiO<sub>2</sub>—35%, PbO—59%, K<sub>2</sub>O—6%) and the material of the substrate was Al<sub>2</sub>O<sub>3</sub>. The measurements were carried out in the temperature range of 775 °C–895 °C with a step of 10 °C. Thirty images were obtained for each temperature. Independent measurements of contact angles were made for each of them. Tables 3 and 4 present average values of the measured angles for individual temperature and their standard deviations, for left and right

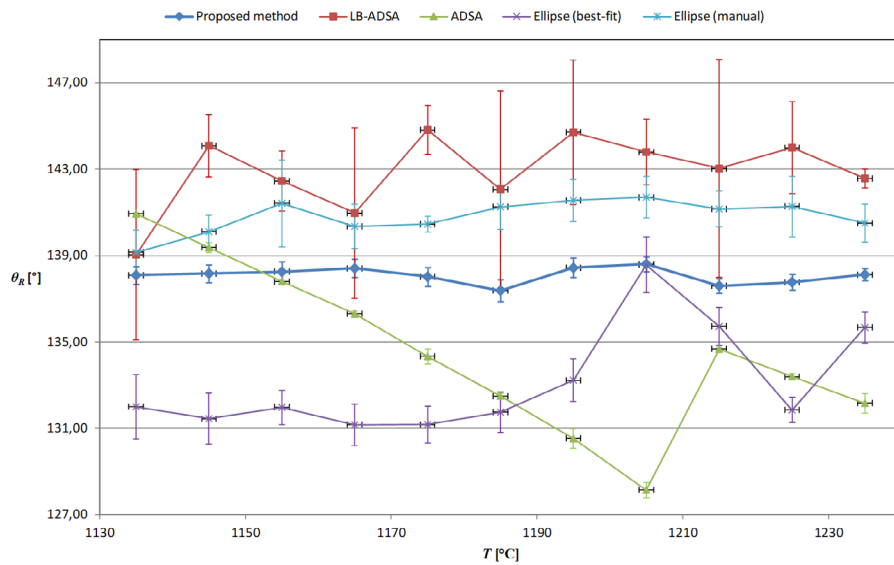


Figure 7. Average values of contact angles for right half-profiles measured in Cu on Al<sub>2</sub>O<sub>3</sub> experiment as function of temperature.

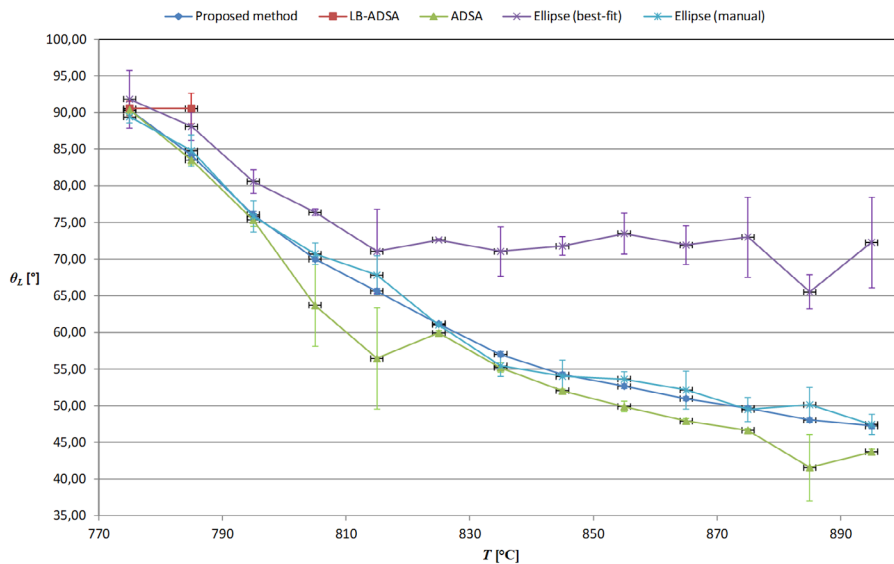


Figure 8. Average values of contact angles for left half-profiles measured in glass on Al<sub>2</sub>O<sub>3</sub> experiment as function of temperature.

half-profiles respectively. Confidence intervals were calculated for average values of contact angles for every temperature and presented as well. Confidence level was assumed 95%. Figure 8 shows the average values of the contact angles for left half-profiles and figure 9 shows the average values of the contact angles for right half-profiles as functions of temperature.

Changes of the contact angle value as a function of temperature are consistent with the expected ones [31, 32]. Low standard deviation values were obtained throughout the entire temperature range. The narrow confidence intervals show that the average values of the contact angle for individual temperature are well estimated. In both experiments, small differences between the values of the contact angle measured for the left and right specimen half-profiles can be observed, possibly because of inhomogeneity of the plate surface, which causes loss of symmetry of the specimen.

### 5. Validation against other methods

In order to validate the proposed algorithm, images acquired during the experiments presented in the previous section were processed using the freely available software implementing popular, widely used methods of determining the contact angle. The results obtained are presented in tables 1–4 and figures 6–9. All calculations were performed on a PC equipped with an Intel i7 processor clocked at 2.4 GHz and 8 GB of RAM.

Figure 10 shows result images obtained with all tested methods for the copper specimen (Cu) on Al<sub>2</sub>O<sub>3</sub> plate at 1195 °C presented in figure 3(a) and 11 shows result images obtained with all tested methods for the glass specimen (SiO<sub>2</sub>—35%, PbO—59%, K<sub>2</sub>O—6%) on Al<sub>2</sub>O<sub>3</sub> plate at 885 °C presented in figure 4(a). Images were cropped to the specimen region for better visualization of the results.

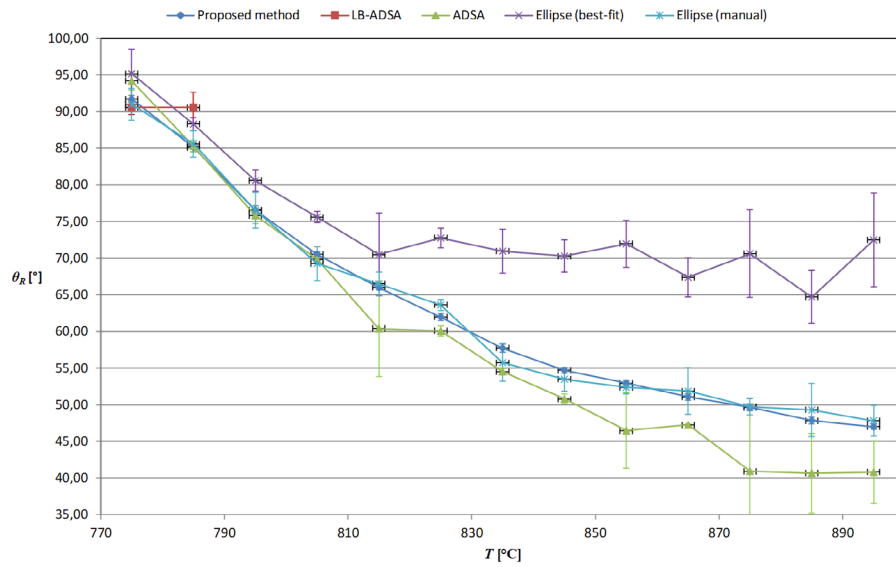


Figure 9. Average values of contact angles for right half-profiles measured in glass on Al<sub>2</sub>O<sub>3</sub> experiment as function of temperature.

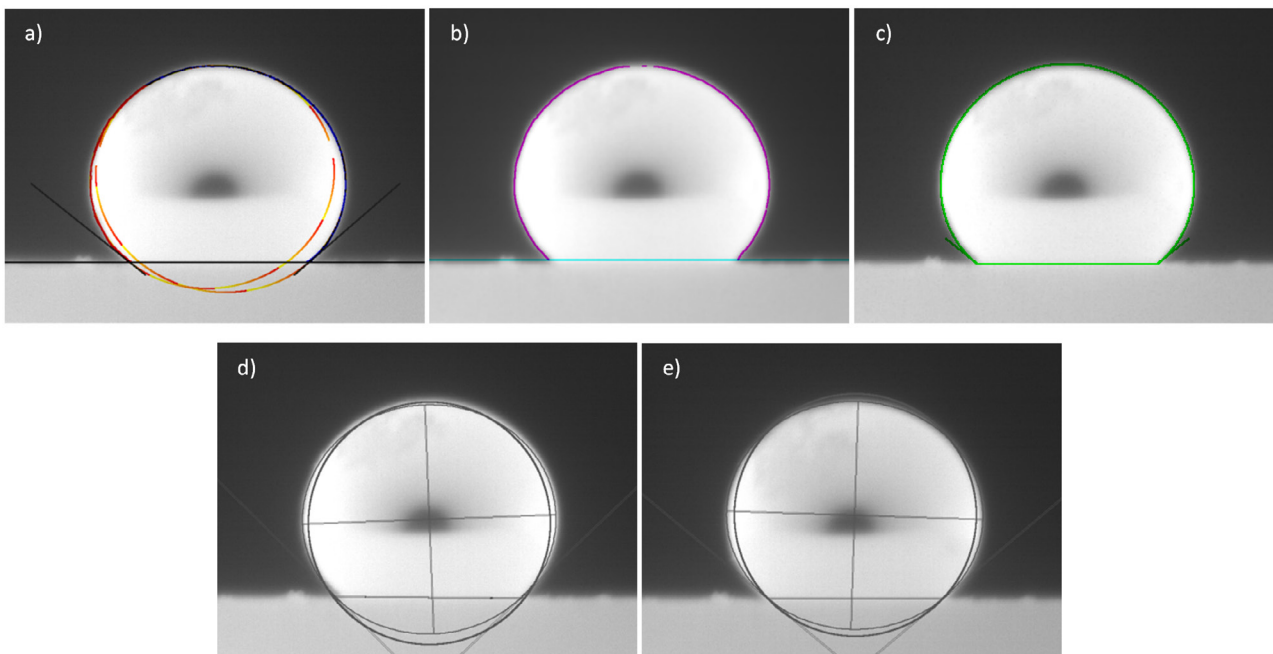


Figure 10. The results of localization of the edges and determination of the contact angles for the copper specimen (Cu) on Al<sub>2</sub>O<sub>3</sub> plate at 1195 °C shown in figure 3: (a) proposed method, (b) ADSA, (c) LB-ADSA, (d) Ellipse (best-fit), (e) Ellipse (manual). Images were cropped to the specimen region for better visualization of the results.

5.1. Axisymmetric drop shape analysis (ADSA)

Axisymmetric drop shape analysis (ADSA) was implemented as part of DropToolKit [17], the computer program written in the Python programming language. Based on the fitting of the Young–Laplace equation to the image data, DropToolKit calculates the interfacial tension and the Young contact angle of the droplet (sessile or pendant). It allows automatic detection of specimen edges by using a modified version of the threshold method. Left and right profiles of the droplet are analysed separately.

The software requires minimal operator participation. It is necessary to provide the correct threshold brightness, enabling

proper separation of the tested sample from the background in the processed image.

DropToolKit was validated against other software packages, including commercial ones [17].

Results obtained using this method are labelled as ‘ADSA’ in tables 1–4 and figures 6–11.

Figure 10(b) and 11(b) show the results of localization of the edges using DropToolKit. Unfortunately, the software does not allow us to generate the resulting images with the determined contact angles marked. It is easy to notice particularly large inaccuracies in the location of the upper edge of the table. Imperfections of the specimen edge detection around the three-phase contact point are also visible, especially for

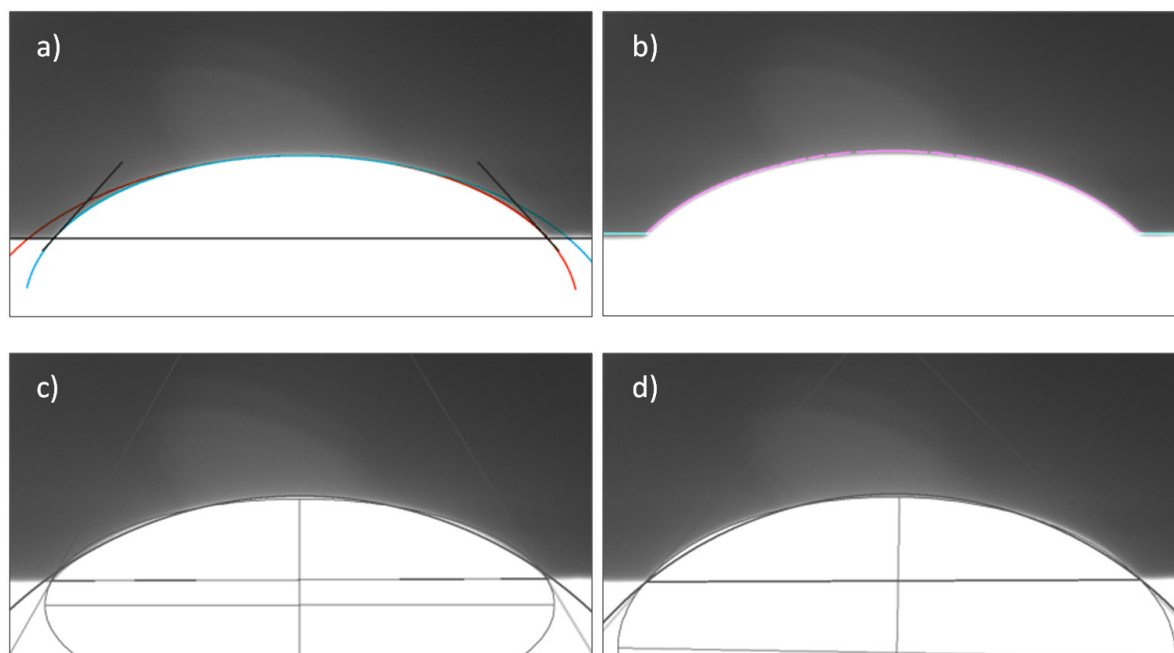


**Figure 11.** The results of localization of the edges and determination of the contact angles for the glass specimen ( $\text{SiO}_2$ —35%,  $\text{PbO}$ —59%,  $\text{K}_2\text{O}$ —6%) on  $\text{Al}_2\text{O}_3$  plate at 885 °C shown in figure 4: (a) proposed method, (b) ADSA, (c) Ellipse (best-fit), (d) Ellipse (manual). Images were cropped to the specimen region for better visualization of the results.

higher contact angle values. This introduces some systematic error and results in large values of the standard deviation for some temperatures (see figures 6–9 and tables 1–4). The influence of lighting conditions on the results obtained is also noticeable. It is particularly visible for the Cu on  $\text{Al}_2\text{O}_3$  experiment in which the contact angle should be constant over the entire temperature range (see figures 6, 7 and tables 1, 2).

The results obtained using DropToolKit software are characterized by lowest values of the standard deviation for most temperatures (see tables 1–4). Unfortunately, they can be affected by some systematic error caused by the selected edge detection method. It is also well known that the ADSA method gives unsatisfactory results in approximation of edges of droplets similar in shape to a sphere [9]. The proposed method is free of these disadvantages.

### 5.2. Low bond axisymmetric drop shape analysis (LB-ADSA)

This model is derived from a first-order perturbation solution of the Laplace equation for axisymmetric drops [21]. Contact angles are obtained considering the whole drop profile. This approximation is computationally much more efficient than a solution obtained from numerical integration (ADSA approach). The drop reflection has been integrated into the drop model for improved detection of the interface position. The drop detection method based on image gradient energy and cubic spline interpolation has been used [22].

The algorithm was implemented in the Java programming language as a plug-in for ImageJ software [21, 22].

Results obtained using this method are labelled as ‘LB-ADSA’ in tables 1–4 and figures 6–11.

Unfortunately, the algorithm requires special operator participation. The average values of brightness of drop and background pixels must be correctly determined and entered. The operator must pre-determine the location and shape of the specimen for each processed image. All this makes the method particularly burdensome and time-consuming.

Figure 10(c) shows the result of localization of the edges and determination of the contact angles using the LB-ADSA method. Imperfections of the specimen edge detection around the three-phase contact point are visible. This introduces some systematic error and results in large values of the standard deviation (see figures 6, 7 and tables 1, 2).

The method is characterized by the highest value of the standard deviation. The used edge detection algorithms did not allow us to correctly locate the samples for the glass on  $\text{Al}_2\text{O}_3$  experiment for contact angles values less than 90 °C. The method assumes the symmetry of the droplets.

The proposed method enables measurement of the full range of contact angle values and provides better determination of the sample profile around the three-phase contact point (see figures 10(a) and 11(a)).

### 5.3. Ellipse approximation

The algorithm calculates the contact angle of a drop on a flat surface using the sphere and the ellipse approximations [23]. In order to calculate the contact angle, four different options are possible: a manual points selection, a measurement by using a circle best-fit, a measurement by using an ellipse best-fit, and an analysis by applying both best-fits.

When the manual points selection is chosen, the user needs to detect the profile manually placing some (at least five) points along the drop edge. The circle and the ellipse passing through the points are reckoned.

In cases of best-fit analysis a manual detection of the base line is required. The operator needs to select a few (at least three) points defining the region with the specimen. The best-fit analysis automatically detects the drop profile. The user has the possibility of modifying the threshold in order to exclude the main part of the background.

The method could fail if the specimen surface is not a straight line.

The algorithm was implemented in the Java programming language as a plug-in for ImageJ software [23].

In tables 1–4 and figures 6–11 results obtained using this method are labelled as ‘Ellipse (best-fit)’ for automatic specimen detection and ‘Ellipse (manual)’ for manual specimen selection.

Figures 10(d) and 11(c) show the results of localization of the edges and determination of the contact angles using the ellipse approximation method with automatic detection of the specimen. Automatic detection of the specimen is rather poor, especially for contact angles values less than 90 °C. It requires the well-defined image and still depends in some way on the subjective evaluation of the operator, who needs to select the points of contact of three phases. The results obtained differ significantly in value from those of other methods (see figures 6–9 and tables 1–4).

Figures 10(e) and 11(d) show the results of localization of the edges and determination of the contact angles using the ellipse approximation method with manual selection of the specimen. Unfortunately, the manual specimen selection requires special operator participation. The operator needs to point the edge of the specimen for each processed image. All this makes the method particularly dependent on subjective operator judgment, and time consuming. The results correspond to those obtained using the proposed method. However, their quality depends on the operator’s skills and experience. The proposed method ensures a fully automated measuring procedure and the results obtained with it are characterized by lower standard deviation values (see tables 1–4).

## 6. Conclusions

Vision-based measurement systems have been used in many industrial applications. Their tasks include acquisition, analysis and processing of images for quantitative description of the recorded scene. The accuracy of this type of measuring instruments depends on the quality of image processing and analysis algorithms. The requirements imposed on the measurement systems stimulate the development and implementation of new algorithms, which presents difficult and interesting challenges.

The new image analysis algorithms presented in this paper allow for fully automatic measurement of the contact angle in a wide temperature range for a variety of materials. The measurement is based on successive approximation of the

specimen edge with ellipses. The obtained results are independent of the subjective assessment of the operator of the measurement system at each stage of the process with high reproducibility.

A feature that distinguishes the proposed algorithm from the others is the combination of the drop edge detection process and determining the contact angle. As a result, it significantly reduces the operator’s participation in the measurement process.

The new algorithm has a number of advantages compared with those existing ones. While ADSA method [9] is often used as a reference, it gives unsatisfactory results for drops similar in shape to a sphere. The proposed algorithm can be successfully applied to samples of various shapes, from spherical (low wettability) to heavily flattened (high wettability) ones. While the ADSA method cannot be used for non-symmetrical samples, the new algorithm allows the measurement of the contact angles of unsymmetrical drops due to the independent approximation of the left and right half-profiles of the specimen in the last stage of the calculation.

As demonstrated by the experiments, the proposed method gives reliable results for images acquired in different conditions and with different levels of distortion. Furthermore, precise positioning of the specimen is not required. The algorithm works well for specimens of different size and localization.

The ADSA method, which is used as a reference, is characterized by high computational complexity, much higher than the proposed one. In addition, it requires a well-defined profile of the specimen, which is usually selected by the system operator.

The main disadvantage of the proposed algorithm is the relatively long processing time, which is significantly longer than in the case of methods based on simple approximation of the sample edge. However, the fact that the measurement process is fully automated makes this disadvantage insignificant.

The new algorithm has been implemented in the THERMO-WET system for measuring surface tension and wetting angles. The experiments were carried out, aimed at the verification of the algorithms, with emphasis on the accuracy of localization and measurement of geometrical parameters of the specimen of the material under investigation, because those have critical impact on the quality of the results obtained.

The use of the above-mentioned method in the THERMO-WET system can improve the quality of acquired images and increase the accuracy and reproducibility of measurements of surface properties.

The measurement results obtained using the developed system are characterized by a much higher accuracy and higher reproducibility, compared with those obtained with the previous time-consuming methods, which depend on the subjective assessments of the operator.

## ORCID iDs

Krzysztof Strzecha  <https://orcid.org/0000-0002-5648-0942>

## References

- [1] Butt H-J, Graf K and Kappl M 2003 *Physics and Chemistry of Interfaces* (New York: Wiley)
- [2] de Gennes P-G, Brochard-Wyart F and Quéré D 2004 *Capillarity and Wetting Phenomena: Drops, Bubbles, Pearls, Waves* (Berlin: Springer)
- [3] Deyev G F and Deyev D G 2006 *Surface Phenomena in Fusion Welding Processes* (Boca Raton, FL: CRC Press)
- [4] Bracco G and Holst B 2013 *Surface Science Techniques* (Berlin: Springer)
- [5] Hartland S 2004 *Surface and Interfacial Tension: Measurement, Theory, and Applications* (New York: Marcel Dekker)
- [6] Ibach H 2006 *Physics of Surfaces and Interfaces* (Berlin: Springer)
- [7] Kwok D Y and Neumann A W 2000 Contact angle interpretation in terms of solid surface tension *Colloids Surf. A* **161** 31–48
- [8] Cwikel D, Zhao Q, Liu C, Su X and Marmur A 2010 Comparing contact angle measurements and surface tension assessments of solid surfaces *Langmuir* **26** 15289–94
- [9] Hoorfar M and Neumann A W 2004 Axisymmetric Drop Shape Analysis (ADSA) for the determination of surface tension and contact angle *J. Adhes.* **80** 727–43
- [10] Li L, Kang W and Ye D 2007 A contact angle measurement method for the droplets in EWOD-based chips 2007 *2nd IEEE Int. Conf. on Nano/Micro Engineered and Molecular Systems* (IEEE) pp 1071–5
- [11] McHale G, Erbil H Y, Newton M I and Natterer S 2001 Analysis of shape distortions in sessile drops *Langmuir* **17** 6995–8
- [12] Atefi E, Mann J A and Taviana H 2013 A robust polynomial fitting approach for contact angle measurements *Langmuir* **29** 5677–88
- [13] Chini S F and Amirfazli A 2011 A method for measuring contact angle of asymmetric and symmetric drops *Colloids Surf. A* **388** 29–37
- [14] Mirzaei M 2017 A new method for measuring the contact angles from digital images of liquid drops *Micron* **102** 65–72
- [15] Ríos-López I, Karamaounas P, Zabulis X, Kostoglou M and Karapantsios T D 2018 Image analysis of axisymmetric droplets in wetting experiments: a new tool for the study of 3D droplet geometry and droplet shape reconstruction *Colloids Surf. A* **553** 660–71
- [16] Biolè D, Wang M and Bertola V 2016 Assessment of direct image processing methods to measure the apparent contact angle of liquid drops *Exp. Therm. Fluid Sci.* **76** 296–305
- [17] Favier B, Chamakos N T and Papathanasiou A G 2017 A precise goniometer/tensiometer using a low cost single-board computer *Meas. Sci. Technol.* **28** 125302
- [18] Sankowski D, Senkara J, Strzecha K and Jezewski S 2001 Automatic investigation of surface phenomena in high temperature solid and liquid contacts *IMTC 2001. Proc. of the 18th IEEE Instrumentation and Measurement Technology Conf. Rediscovering Measurement in the Age of Informatics (Cat. No.01CH 37188)* vol 2 (IEEE) pp 1397–400
- [19] Strzecha K and Koszmider T 2008 Drop shape analysis for measurements of surface tension and wetting angle of metals at high temperatures 2008 *Int. Conf. on Perspective Technologies and Methods in MEMS Design* (IEEE) pp 57–9
- [20] Strzecha K 2016 *Selected Algorithms of Quantitative Image Analysis of Measurements of Properties Characterizing Interfacial Interactions at High Temperatures* (Lodz: University of Technology Press)
- [21] Stalder A F, Melchior T, Müller M, Sage D, Blu T and Unser M 2010 Low-bond axisymmetric drop shape analysis for surface tension and contact angle measurements of sessile drops *Colloids Surf. A* **364** 72–81
- [22] Stalder A F, Kulik G, Sage D, Barbieri L and Hoffmann P 2006 A snake-based approach to accurate determination of both contact points and contact angles *Colloids Surf. A* **286** 92–103
- [23] Williams D, Kuhn A, Amann M, Hausinger M, Konarik M and Nesselrode E 2010 Computerized measurement of contact angles *Galvanotechnik* **101** 2502–12
- [24] Strzecha K, Fabijanska A, Koszmider T and Sankowski D 2014 Selected algorithms of quantitative image analysis for measurements of properties characterizing interfacial interactions at high temperatures *Computer Vision Research in Robotics, Process Tomography, Medical and Industrial Applications* ed D Sankowski (Singapore: World Scientific) pp 339–82
- [25] Fabijańska A and Sankowski D 2009 Improvement of the image quality of a high-temperature vision system *Meas. Sci. Technol.* **20** 104018
- [26] Strzecha K, Koszmider T, Zarebski D and Lobodzinski W 2012 Passive auto-focus algorithm for correcting image distortions caused by gas flow in high-temperature measurements of surface phenomena *Image Process. Commun.* **17** 379–84
- [27] Yoo T S 2004 *Insight into Images: Principles and Practice for Segmentation, Registration, and Image Analysis* (Natick: A K Peters)
- [28] Zhang Y-J 2006 *Advances in Image and Video Segmentation* (London: IRM Press)
- [29] Gonzalez R C and Woods R E 2008 *Digital Image Processing* (Englewood Cliffs, NJ: Prentice-Hall)
- [30] Canny J 1986 A computational approach to edge detection *IEEE Trans. Pattern Anal. Mach. Intell.* **PAMI-8** 679–98
- [31] Scheu C, Klein S, Tomsia A P and Ruhle M 2002 Chemical reactions and morphological stability at the Cu/Al<sub>2</sub>O<sub>3</sub> interface *J. Microsc.* **208** 11–7
- [32] Eustathopoulos N 2015 Wetting by liquid metals—application in materials processing: the contribution of the Grenoble Group *Metals* **5** 350–70